

MAY 02 2023

The effect of source backing materials and excitation pulse durations on laser-generated ultrasound waveforms

Srinath Rajagopal; Thomas Allen; Martin Berendt; ... et. al



J Acoust Soc Am 153, 2649 (2023)

<https://doi.org/10.1121/10.0019306>



CrossMark





Advance your science and career
as a member of the

ACOUSTICAL SOCIETY OF AMERICA

LEARN MORE



The effect of source backing materials and excitation pulse durations on laser-generated ultrasound waveforms

Srinath Rajagopal,^{1,a)}  Thomas Allen,² Martin Berendt,³ Di Lin,^{3,b)} Shaif-ul Alam,³ David J. Richardson,³ and Ben T. Cox² 

¹Ultrasound and Underwater Acoustics, National Physical Laboratory, Hampton Road, Teddington, TW11 0LW, United Kingdom

²Department of Medical Physics and Biomedical Engineering, University College London, Malet Place Engineering Building, Gower Street, London, WC1E 6BT, United Kingdom

³Optoelectronics Research Centre, University of Southampton, Southampton, SO17 1BJ, United Kingdom

ABSTRACT:

In this article, it is shown experimentally that a planar laser-generated ultrasound source with a hard reflective backing will generate higher acoustic pressures than a comparable source with an acoustically matched backing when the stress confinement condition is not met. Furthermore, while the source with an acoustically matched backing will have a broader bandwidth when the laser pulse is short enough to ensure stress confinement, the bandwidths of both source types will converge as the laser pulse duration increases beyond stress confinement. The explanation of the results is supported by numerical simulations. © 2023 Author(s). All article content, except where otherwise noted, is licensed under a Creative Commons Attribution (CC BY) license (<http://creativecommons.org/licenses/by/4.0/>).

<https://doi.org/10.1121/10.0019306>

(Received 26 August 2022; revised 14 April 2023; accepted 14 April 2023; published online 2 May 2023)

[Editor: Julian D Maynard]

Pages: 2649–2658

I. INTRODUCTION

To generate a laser-generated ultrasound (LGUS) pulse via the *photoacoustic effect*, a short duration laser pulse is directed onto an optically absorbing material. Briefly, the physical process of the photoacoustic effect is as follows. The absorption of the photons and their subsequent thermalisation leads to rapid heating of the absorbing region. If the heating is so fast that the density has no time to change, i.e., *isochoric* thermalisation, then the rise in pressure that accompanies the rise in temperature occurs under a condition is known as *stress confinement*. The pressure rise has been modelled as the initial acoustic pressure distribution because it acts as a source of acoustic waves. The temperature rise will diffuse to the surrounding cooler regions, although on a slower time scale than the acoustic propagation.¹ However, metals are an exception² due to their very short absorption depth (<10 nm) and high thermal diffusivity (e.g., the thermal diffusivity of aluminium² is at least two orders greater in magnitude than polymers³) which causes temperature to diffuse away at a much faster rate from the absorption region than acoustic propagation.

A useful condition that indicates whether or not stress confinement has occurred can be found by comparing the duration of the laser pulse, τ , with the stress relaxation time, $\tau_{ac} = \min(\mu^{-1}, d)/c$, where c [m s⁻¹] is the sound-speed, μ^{-1} [m] is the optical penetration depth, and d the optical

absorber thickness. When $\tau \ll \tau_{ac}$, the localized pressure increase does not have time to completely propagate out of the deposition region whilst energy is being deposited, and so the acoustic pressure amplitude will be maximized under this condition. If the stress confinement condition is not met, $\tau > \tau_{ac}$, the acoustic pressure due to the early arriving part of the laser pulse will have left the absorbing region before the latter parts are thermalized; the acoustic pressure spreads out, rather than builds up, and therefore, for the same total amount of energy, the maximum amplitude decreases as the laser pulse duration increases. Similarly, thermal confinement time can be checked using the relation (1D) given by $\tau_{th} = 1/(4\chi\mu^2)$, where χ [m² s⁻¹] is the thermal diffusivity.² For example, consider $\chi = 1.1 \times 10^{-7}$ m² s⁻¹ and $c = 1050$ m s⁻¹ for polydimethylsiloxane (PDMS) polymer^{4,5} and $\mu = 68\,000$ m⁻¹ for PDMS-based carbon polymer nanocomposite,⁶ τ_{ac} and τ_{th} are approximately 14 ns and 490 μ s, respectively. It is clear that for polymer nanocomposites stress confinement is a more stringent condition to satisfy over thermal confinement.

Several nanocomposite-based source materials have been developed over the last two decades to improve the conversion efficiency of optical energy to acoustic energy.^{6–13} The aim, in some cases, was to generate high pressure and broadband ultrasound pulses targeted at a range of biomedical applications including both imaging and therapy.^{14,15} Such advancements facilitated the development of a portable LGUS device that generates a short (broadband) planar ultrasound pulse with an amplitude of several MPa to assist with the calibration of hydrophones up to 100 MHz.¹⁶

^{a)}Electronic mail: srinath.rajagopal@npl.co.uk

^{b)}Current address: School of Information Engineering and Guangdong Provincial, Key Laboratory of Photonics Information Technology, Guangdong University of Technology, Guangzhou, 510006, China.

A common method for fabricating LGUS sources is by depositing a thin optically absorbing layer on an acoustically hard-reflective transparent backing material such as glass plate, optical lens, or the tip of an optical fibre. Consider the stress-confined case of a short laser pulse incident on the absorbing layer from the backing side. In this case, the resulting initial acoustic pressure profile will resemble the profile of the absorbed optical energy. This initial acoustic pressure will subsequently divide into two equal parts: one wave propagating towards the hard-reflective backing (back-going, say) and the other wave towards the medium into which it is coupled (front-going), for example, water [see Fig. 1(b)]. A proportion of the back-going wave will be reflected and immediately follow the front-going wave. On the other hand, if, rather than being reflective, the backing material were acoustically identical to the absorbing layer and thick enough such that there was no reflection, then only the front-going wave would propagate into the water. Therefore, the acoustic pulse generated from an optically absorbing layer backed by an acoustic reflector will be twice as long as that of a source with a backing acoustically matched to the absorbing layer. However, because of stress confinement, the maximum amplitude with and without the reflection will be the same.^{17,18} Interestingly, it was discovered in a previous experimental study that the acoustic pressure amplitude generated by such a carbon-polymer nanocomposite (CPN) source does in fact depend significantly on whether it was deposited on a hard-reflective backing (glass) or an acoustically matched polymer backing.¹⁹ A plausible explanation of this effect is that when the laser pulse is longer than the stress confinement requirement, the back-going wave will be reflected by the glass, back to the front during the continued optical deposition of heat and there will be a consequent build-up of pressure in the absorbing region, the amplitude of which will be determined by both the reflection and the heating. If the amplitude polarity of the reflected wave is the same as the incident wave, the total acoustic pressure reached will be higher than it would be in the absence of the reflection.

In Ref. 20, this explanation was investigated theoretically. An analytical time-domain solution was derived for the acoustic pressure waveform generated by a planar optical ultrasound source (medium B) sandwiched between a backing (medium A) on one side and a second medium (medium C) on the other, e.g., water (see Fig. 1). It was shown that by varying the optical attenuation coefficient, μ [m^{-1}] (inverse of optical penetration depth), the thickness of the absorbing layer, the acoustic properties of the backing and absorbing layers, and the laser pulse duration, a wide variety of pulse shapes and trains can be generated. It was also shown that when stress-confinement is not satisfied, using a reflective backing generated pulses with a higher amplitude than using an acoustically matched backing under otherwise identical conditions, as hypothesised. Furthermore, the model predicted that the ratio of the amplitudes in the reflective and matched cases increases

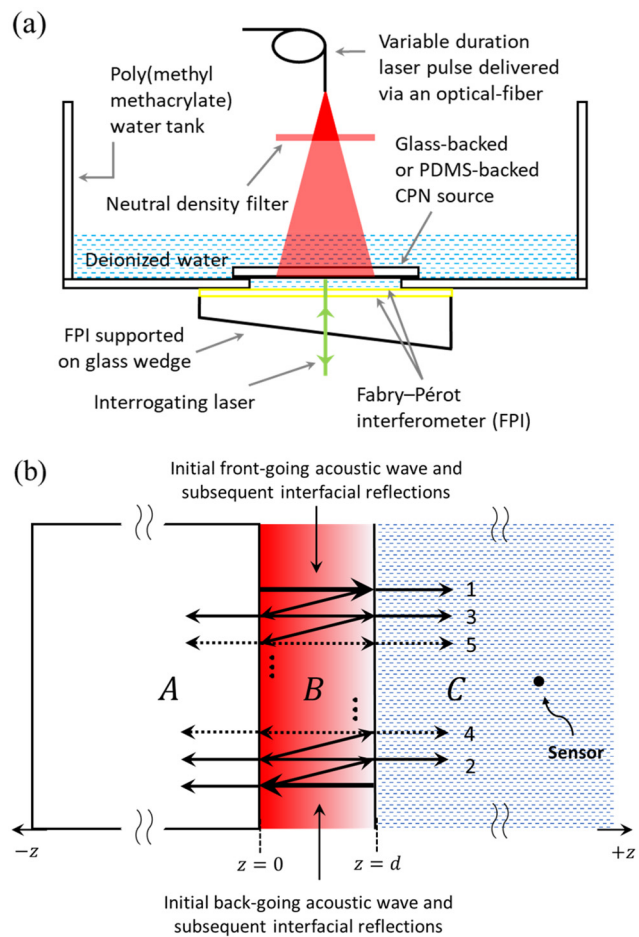


FIG. 1. (Color online) The schematics are not to scale. (a) Measurement setup used to test the effect of source backing material on LGUS from glass-backed and PDMS-backed CPN sources. A variable-duration fibre laser was used to generate laser pulses of FWHM duration from 10 to 200 ns. A Fabry-Pérot Interferometer (FPI) was used to record the acoustic pressure times-series generated by the CPN source. (b) The backed CPN source in (a) is shown in an exploded view and is oriented by 90° . Medium A, B, and C are the glass or PDMS-backing, CPN source and water, respectively and d is the thickness of the CPN source. The laser pulse entering from optically transparent medium A is absorbed in medium B. The front-going and back-going acoustic waves and their subsequent interfacial reflections are shown separately for clarity. For longer laser pulses ($\tau \gg \tau_{ac}$) and if the CPN is backed with a hard-reflecting material then all the back-propagating interfacial reflections at the interface of medium A and medium B propagate back into medium B. During the continued optical deposition of heat, these waves will constructively add-up to produce more pressure compared to a CPN with matched backing. The FPI sensor records the waves propagating in medium C. If the thickness of medium A is finite then the fractional waves that reach the end of medium A boundary (towards $-z$) will also undergo interfacial reflections before arriving at medium B and well after optical heating time. This process continues until all waves are lost via interfacial effects and acoustic absorption in different media.

monotonically with laser pulse duration τ until it reaches a limiting value, which is dependent on acoustic properties of absorber and backing.

In this paper, this prediction of a monotonic increase to a limit will be examined experimentally using a fibre laser whose pulse duration can be varied over a wide range (Sec. II). These measurements will be qualitatively compared to a

numerical model that is a generalisation of the analytical model in Ref. 20 (Sec. III).

II. EXPERIMENTAL MEASUREMENTS

A. Tests using a tunable duration fibre-laser

The variable-duration pulsed fibre laser system²¹ used in the experiments is based on a master oscillator power amplifier configuration, which consists of the output of a seed laser amplified by a chain of ytterbium-doped fibre amplifiers. Such a configuration provides the ability to easily scale the output power of the laser by adding more amplifiers, but also supports the capability of shaping the excitation pulses, as the output of the fibre laser follows the shape provided by the seed laser. The custom-designed fibre laser system was comprised of a super luminescent diode as a seed source and a cascade of four ytterbium-doped fibre amplifier stages. The final amplification stage used a custom-drawn large core diameter (200 μm) fibre to obtain pulse energies of up to 10 mJ. The system provided variable pulse durations (10–500 ns) and pulse repetition frequencies (100 Hz to 1 kHz), and the emission wavelength was 1064 nm.

The measurement setup consisting of the fibre laser and Fabry–Pérot interferometric (FPI) ultrasound sensor²² is shown schematically in Fig. 1. The thickness of the mirrored polymer cavity forming the FPI sensor was nominally 22 μm , which was previously shown to exhibit a smooth frequency response with -6 dB bandwidth of at least 50 MHz and the spot diameter of the interrogating laser was 64 μm . The distance between the CPN sources and the FPI sensor was approximately 4.9 mm. The laser beam diameter incident on the CPN sources was around 2 cm, the pulse energy at the output of the fibre was 8 mJ for all pulse durations and the pulse repetition frequency was 100 Hz. After transmission through a 50% neutral density filter, the laser fluence at the source location was less than 1.5 mJ cm^{-2} . The neutral density filter was used to limit the number of unabsorbed photons reaching the FPI, which would otherwise cause the FPI signal to fluctuate due to interaction of the excitation and interrogating lasers. Measurements were taken at five pulse durations of 10, 20, 50, 100, and 200 ns. The sampling rate of the digitizer attached to the FPI sensor instrumentation was 200 MHz. The acquired signal consisted of 1600 samples, which corresponds to an acquisition duration of 8 μs . Also, a measurement was made on a different experimental setup⁶ using a 4 ns duration laser at 2 mJ cm^{-2} . This setup (described in Ref. 6) employed a 0.4 mm diameter membrane hydrophone calibrated up to 60 MHz, which assisted in estimating the peak pressures²³ of LGUS pulses generated from glass-backed and polydimethylsiloxane (PDMS) backed sources under the stress confinement condition. The source-hydrophone separation was 5.2 mm.

B. Carbon-polymer nanocomposite sources

The carbon-polymer nanocomposite (CPN) was prepared by mechanically dispersing carbon nanotubes (CNT) in a bulk polymer matrix, in this case polydimethylsiloxane

(PDMS). In a previous study, the optical attenuation coefficient for a 1.25 wt. % CNT dispersed in PDMS was measured as 68 000 m^{-1} .⁶ Using the known sound-speed of PDMS, for a 10:1 (elastomer:curing agent) mixture it is nominally 1050 m s^{-1} ,⁵ the relaxation time $\tau_{ac} = 1/\mu c \approx 14$ ns. Since this stress relaxation time is greater than the shortest pulse duration of the variable duration fibre laser, this weight percentage was chosen for fabricating acoustically reflecting and matched-backing sources. The details of the CPN source fabrication can be found in Refs. 6 and 24. Here, only the important details relevant to this study are provided.

The reflecting CPN source was fabricated on laboratory grade glass (Corning) slides of dimensions 75 mm \times 50 mm \times 1 mm (*length* \times *width* \times *thickness*). A freshly prepared CPN paste was coated on the glass slide using a height-adjustable blade film applicator controlled by a digital micrometre. The coated glass slide was oven-cured at 100 $^{\circ}\text{C}$ for 35 min to complete the fabrication. To fabricate matched-backed sources, the following approach was taken. A small amount of debonding agent (petroleum jelly) was spread on one surface of the glass slides. The surface was then wiped off using lens cleaning tissue, which leaves a film sufficiently thin to be effectively parallel to the surface of the glass. A thin layer of the CPN mixture was coated on top of the debonding agent using the blade film applicator. The glass slides with their coated surface facing up were placed in a non-stick baking tray whose insides was also coated with debonding agent. The tray was then filled with a 5:1 ratio of PDMS:catalyst mixture approximately to a height of 2–3 mm above the glass slide. During curing, the debonding agent prevents the CPN film sticking to glass and instead ensures that it bonds to the PDMS-catalyst mixture forming a PDMS-backed source. After allowing the tray to return to laboratory temperature, the contents of the tray can be freed. The embedded glass slides and the PDMS-backed sources were removed using a scalpel and cut to the lateral dimensions of the glass slide. Four glass-backed and four PDMS-backed sources were fabricated.

C. Thickness estimate of CPN coatings

The coating thickness of the glass-backed sources was determined by measuring the glass slide alone and then the glass slide with the cured coating at six sites using a 1 μm resolution digital screw gauge. The coating thickness of PDMS-backed sources cannot be measured in a similar way due to the fabrication process involved, and therefore, the thicknesses were derived indirectly using an optical method, as follows. The wavelength-dependent (unitless) optical absorbance, $A_o(\lambda)$, of the glass-backed and PDMS-backed sources was measured using a spectrophotometer (400–900 nm, Lambda 800, Perkin Elmer, Waltham, MA, USA). The optical absorbances of CPN sources were measured, three times each, near to the central region of the coating over an area of 5 \times 5 mm.

The optical attenuation coefficient, $\mu_{CPN}(\lambda)$, of each glass-backed source was determined using the relation

$$\mu_{CPN}(\lambda) = \frac{A_o(\lambda) \times \ln 10}{d_{th}}, \quad (1)$$

where d_{th} is the measured thickness of the CPN coating on the glass slide.

The error $\Delta\mu_{CPN}(\lambda)$ in the calculation of $\mu_{CPN}(\lambda)$ was determined using the relation

$$\Delta\mu_{CPN}(\lambda) = \sqrt{\left[\frac{\sigma\{A_o(\lambda)\}}{A_o(\lambda)}\right]^2 + \left[\frac{\sigma\{d_{th}\}}{d_{th}}\right]^2}, \quad (2)$$

where $\sigma\{A_o(\lambda)\}$ is the experimental standard deviation calculated from three set of repeat measurements and $\sigma\{d_{th}\}$ is the experimental standard deviation calculated from six set of measurements across six sites on the CPN.

Finally, a weighted mean, $\bar{\mu}_{CPN}$ and weighted uncertainty, $u(\bar{\mu}_{CPN})$ were computed as follows:

$$\bar{\mu}_{CPN} = \frac{\sum_i^n \frac{\mu_{CPN}(i)}{\Delta\mu_{CPN}^2(i)}}{\sum_i^n \frac{1}{\Delta\mu_{CPN}^2(i)}} \quad (3)$$

and

$$u(\bar{\mu}_{CPN}) = \sqrt{\frac{1}{\sum_i^n \frac{1}{\Delta\mu_{CPN}^2(i)}}}, \quad (4)$$

where $i = 1, 2, \dots, n$.

In Table I, results from 600 nm wavelength measurement are listed. The use of the weighted approach can be justified because (i) there is no significant difference between the arithmetic mean (60 mm^{-1}) and weighted mean (61 mm^{-1}), (ii) errors, $\Delta\mu_{CPN}(\lambda)$ from four samples are not significantly different to each other, (iii) standard uncertainty from our values of μ_{CPN} ($\sigma = 2.5 \text{ mm}^{-1}$) is not significantly different to weighted uncertainty ($u = 2.9 \text{ mm}^{-1}$), and (iv) all four values of μ_{CPN} and their errors $\Delta\mu_{CPN}$ overlap. It should be noted that much of the error contribution in $\Delta\mu_{CPN}(\lambda)$ arises from the thickness estimates of CPN layer

on glass-backed sources. For comparison, the worst-case sample variance was 19 parts per thousand for thickness and 99 ppm for absorbance. It would have been possible to reduce the error to a lower value if a sub-micron resolution screw gauge were available.

The thickness of each PDMS-backed source can be indirectly obtained by substituting the respective optical absorbance value, $A_o(\lambda)$ and $\bar{\mu}_{CPN} = 61 \pm 3 \text{ mm}^{-1}$ in Eq. (1) and the associated error can be calculated using Eq. (2). The results are summarized in Table II. There is a small measurement bias in deriving the coating thickness of PDMS-backed sources due to, first, the optical loss within the clear PDMS backing and, second, the difference between the refractive indices of glass and PDMS. To check the significance of the former, the optical absorbance was measured for two rectangularly cast PDMS blocks of two different thicknesses of size $10 \text{ mm} \times 20 \text{ mm}$ (*width* \times *height*). The means and experimental standard deviations from 15 measurements across different sites of the two samples were $4.26 \pm 0.02 \text{ mm}$ and $7.64 \pm 0.02 \text{ mm}$. The means and experimental standard deviations from eight measurements of optical absorbances on different sites of the samples at 600 nm of thin and thick PDMS blocks were 0.045 ± 0.001 and 0.058 ± 0.001 , respectively. By measuring the difference in absorbance between PDMS blocks of different thicknesses, the effect of interfacial loss can be removed. The difference in both the optical absorbance and thickness from the two PDMS blocks were used to calculate μ_{PDMS} and associated $\Delta\mu_{PDMS}$ was calculated by combining standard deviations which was found to be $9 \pm 1 \text{ m}^{-1}$ at 600 nm. The second bias arises from the difference in refractive indices of glass and PDMS, which are 1.5095 and 1.4297,²⁵ respectively, at 600 nm, a 5.3% difference. However, the relative difference in the optical intensity reflection of glass and PDMS interfaced to air, which is the case during spectrophotometer measurements, is only 1%. The magnitude of these two biases are small and hence no correction was applied to the estimated thicknesses of CPN coating on PDMS-backed sources.

The two PDMS-backed sources with a same thickness of $23 \pm 2 \mu\text{m}$ had some gaps in the coating regions and hence were not suited for the experiment. Therefore, for final set of LGUS measurements two glass-backed sources

TABLE I. Measured optical absorbances $A_o(\lambda)$ at 600 nm and thicknesses of CPN coating on glass slides together with their experimental standard deviations were used in the estimation of a weighted mean and its uncertainty of the optical absorption coefficient of the CPN material.

| Glass-backed CPN source No. | Mean thickness, d_{th} [μm] | Experimental standard deviation, $\sigma(d_{th})$ [μm] | Mean optical absorbance, $A_o(\lambda)$ ^a | Experimental standard deviation, $\sigma(A_o)$ ^b | μ_{CPN} [mm^{-1}] | $\Delta\mu_{CPN}$ [mm^{-1}] |
|--|--|---|--|---|----------------------------------|--|
| 1 | 24 | 2 | 0.687 | 0.004 | 66 | 6 |
| 2 | 26 | 2 | 0.693 | 0.007 | 61 | 5 |
| 3 | 24 | 3 | 0.570 | 0.002 | 54 | 7 |
| 4 | 20 | 2 | 0.507 | 0.004 | 58 | 7 |
| Weighted mean, $\bar{\mu}_{CPN}$ | | | | | 61 | |
| Weighted uncertainty, $u(\bar{\mu}_{CPN})$ | | | | | 3 | |

^aThe spectrophotometer outputs $A_o(\lambda)$ data with up to six decimal places, which was rounded to three after the means were calculated.

^bThe calculated $\sigma(A_o)$ was rounded to three decimal places.

TABLE II. Estimated thicknesses of CPN coating on PDMS-backed sources. Measured optical absorbances $A_o(\lambda)$, of PDMS-backed CPN source at 600 nm and optical absorption coefficient, $\bar{\mu}_{CPN}$ of CPN coating on glass-backed slides together with their respective experimental standard deviations and errors were used in the estimation CPN coating thicknesses on PDMS-backed sources.

| PDMS-backed CPN source No. | Mean optical absorbance, $A_o(\lambda)^a$ | Experimental standard deviation, $\sigma(A_o)^b$ | $\bar{\mu}_{CPN}$ obtained from glass-backed CPN [mm^{-1}] | Uncertainty, $u(\bar{\mu}_{CPN})$ [mm^{-1}] | Estimated thickness, d_{th} [μm] | Δd_{th}^c [μm] |
|----------------------------|---|--|---|--|---|-------------------------------------|
| 1 | 0.539 | 0.003 | 61 | 3 | 20 | 2 |
| 2 | 0.622 | 0.008 | | | 23 | 2 |
| 3 | 0.617 | 0.016 | | | 23 | 2 |
| 4 | 0.525 | 0.024 | | | 20 | 2 |

^aThe spectrophotometer outputs $A_o(\lambda)$ data with up to six decimal places, which was rounded to three after the means were calculated.

^bThe calculated $\sigma(A_o)$ was rounded to three decimal places.

^cThe error values were rounded up to the next largest integer value.

($24 \pm 2 \mu\text{m}$) and two PDMS-backed sources ($20 \pm 2 \mu\text{m}$), were selected for the experiments. These two thicknesses are larger than the optical penetration depth, $1/\bar{\mu}_{CPN} \approx 16 \mu\text{m}$. Sample glass-backed and PDMS-backed sources are shown in Fig. 2.

D. Experimental and numerical results

The peak-positive pressures estimated using the calibrated hydrophone in the 4 ns laser pulse setup from glass-backed and PDMS-backed sources were 123 and 90 kPa, respectively. These pressures are low, and no wave steepening was observed in the hydrophone measurements, suggesting that any effects of nonlinear propagation were negligible. The acoustic pressure time-series generated by the glass-backed and PDMS-backed CPN sources are shown in Fig. 3 along with the results from the numerical model (Sec. III) for comparison. As can be seen, when stress

confinement is not met, the acoustic pulse is more spread out, and the pressure amplitude decreases with increasing laser pulse duration. The acoustic time-series are time-gated to eliminate the interfacial reflections arising from the finite thickness of the backing medium of the CPN sources.¹⁶ The time-series were windowed using a Kaiser window ($\alpha = 9$) before calculating the Fourier spectra shown in Fig. 4.

The ratios calculated using the peak-positive amplitudes of the glass-backed over PDMS-backed sources are shown in Fig. 5 including the ratio calculated from the 4 ns measurements. Also, plotted in Fig. 5 are the amplitude ratios from the numerical simulations at distances of 3.4, 4.9, and 6.4 mm from the source (see Sec. III for details on modeling), which was to mainly see if there was a dependence of ratios with propagation distance. The experimental ratios at 4 and 10 ns are nearly identical, which suggests that there is stress confinement at these pulse durations. However, when there is stress confinement, the pressure amplitudes from the glass-backed and PDMS-backed sources might be expected to be equal [this is the prediction of the analytical model (Ref. 20)], but this is not the case. The difference is the presence of acoustic absorption. There is more high-frequency content in the shorter PDMS-backed pressure pulse compared to the longer glass-backed pulse, which includes a reflection from the backing (see Fig. 3). The preferential loss of high frequencies both in CPN and water therefore causes the amplitude to decrease more rapidly for the PDMS-backed source. This is consistent with the fact that the simulated results also show this effect with a small increase with distances from the source. Simulations were also repeated by allowing nonlinear propagation in the water medium, but no noticeable differences were found in the results shown in Fig. 5. This suggests that nonlinear propagation was negligible as the pressure amplitudes are sufficiently low.

The -6 dB bandwidth ratios calculated from the amplitude spectra of PDMS-backed over glass-backed sources from experiment and numerical time-series are shown in Fig. 6. When the laser pulse durations are less than the stress confinement time (14 ns), then the gain in -6 dB bandwidth from PDMS-based sources is significant compared to glass-backed sources. As the laser pulse durations increase, the

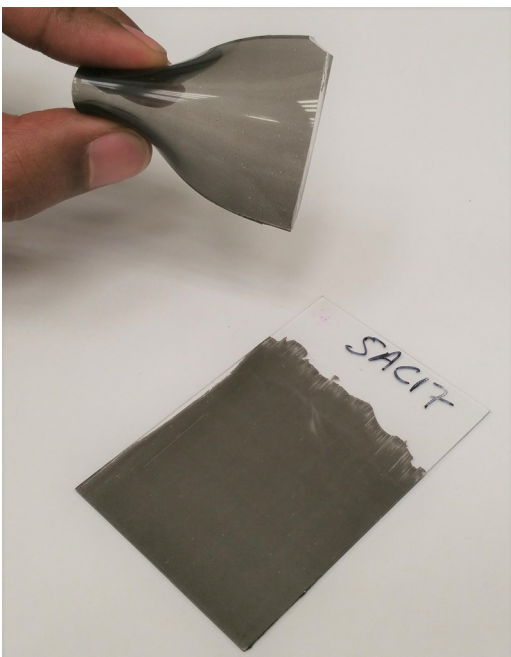


FIG. 2. (Color online) PDMS-backed (top) and glass-backed (bottom) CPN sources made with 1.25 wt. % CNT. The PDMS-backed source is not rigid and can be flexed, as shown. The thicknesses of the CPN coatings on glass and PDMS backings were $24 \pm 2 \mu\text{m}$ and $20 \pm 2 \mu\text{m}$, respectively.

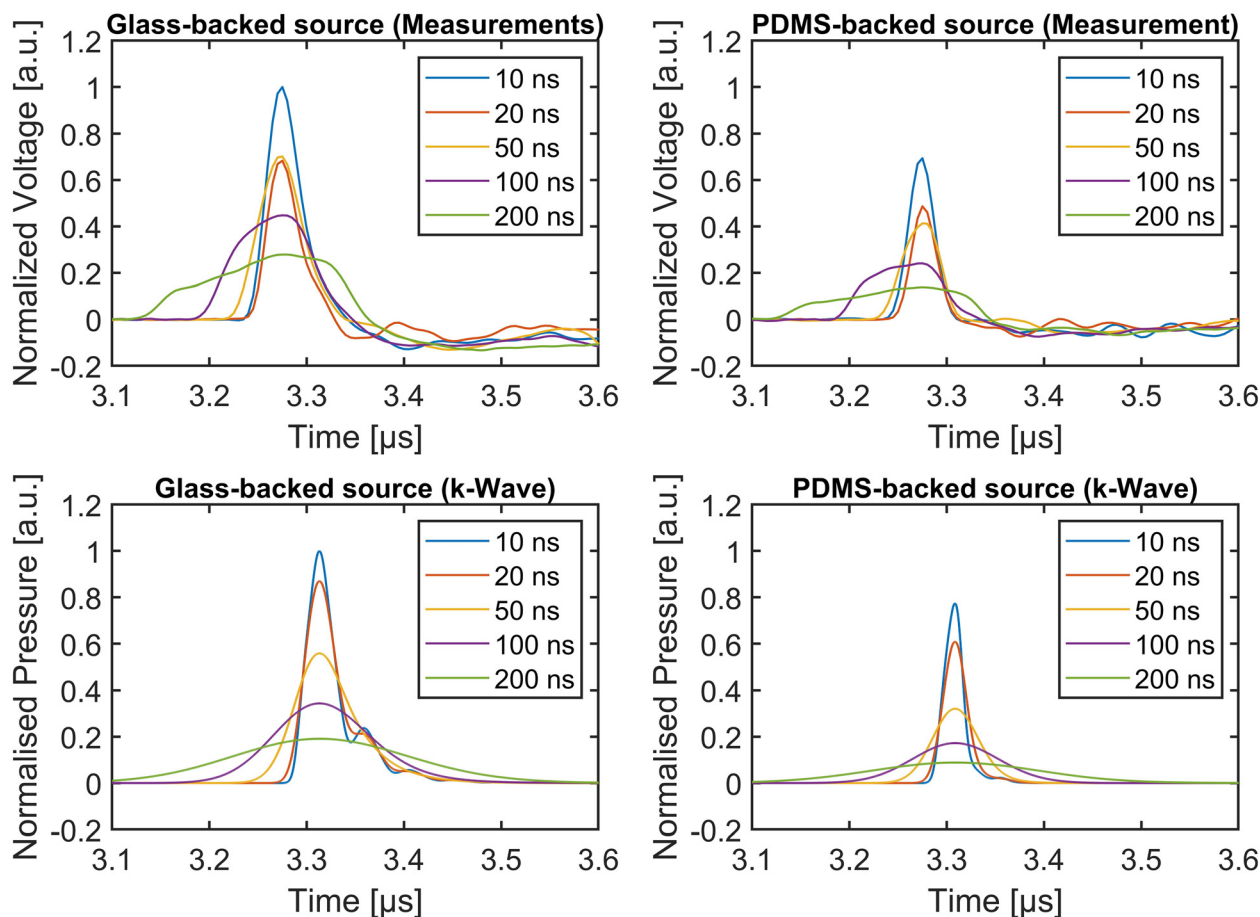


FIG. 3. (Color online) (Top row) Measured sensor voltage time-series acquired from glass-backed and PDMS-backed CPN sources. (Bottom row) Simulated pressure time-series from glass-backed and PDMS-backed sources using the numerical model described in Sec. III. The voltage and pressure waveforms were normalized using respective amplitudes of the measured and simulated glass-backed CPN source waveforms of 10 ns laser pulse duration. The amplitude polarity change in the trailing part of the pulses in the measured waveforms is due to the acoustic diffraction arising from the Gaussian profile in the spatial extent of the excitation laser beam (Ref. 26), whereas the numerical simulations were performed in 1D, which assumes a perfectly planar wavefront.

relative difference in the pulse duration of the pressure pulses from both glass-backed and PDMS-backed sources become smaller and consequently their -6 dB bandwidths converge to the same value. However, since the amplitudes of the pressure pulses in the glass-backed case are always higher than the PDMS-backed case, the spectral pressure amplitudes are also higher in the glass-backed case (see Fig. 4). Although the qualitative agreement between experiment and numerical results in Fig. 6 is clear, the imperfect quantitative agreement may be due to inaccuracies in the CPN acoustic absorption values assumed in the model or those obtained from the literature.

III. NUMERICAL ACOUSTIC MODEL

This section will describe the model used to obtain the numerical results shown in the figures in Sec. II. The analytical model described in Ref. 20 was not used as it made three assumptions that may not be true for the experimental arrangement described above. First, the laser pulse was modelled as rectangular in time, when here it is closer to Gaussian. Second, acoustic absorption was assumed

negligible, but at the frequencies encountered here that seems unlikely to be the case for most materials. Third, the propagation was assumed to be linear, but it has been shown previously that nonlinear propagation can be significant for LGUS sources.⁶ (Although, here the nonlinearity was shown to be negligible, as mentioned later, the nonlinear model was used to confirm the results.) For these reasons, a numerical model that accounts for acoustic absorption and nonlinear propagation, and allows arbitrary pulse shapes, was used here for comparison to the experimental measurements.

k-Wave, a MATLAB[®] toolkit, is an acoustic wave solver that uses a k-space pseudospectral method.^{27–29} The model was divided into two steps: first, the source generation within the CPN, reflections within the source region, and initial propagation into the water and, second, the remaining propagation through the water to the position of the detector. Because of the homogeneous medium and lower frequency content in step 2, that part of the simulation converged with a larger grid spacing than step 1, making the simulation computationally much more efficient. In step 1, the model included three layers: glass or PDMS backing, PDMS-based

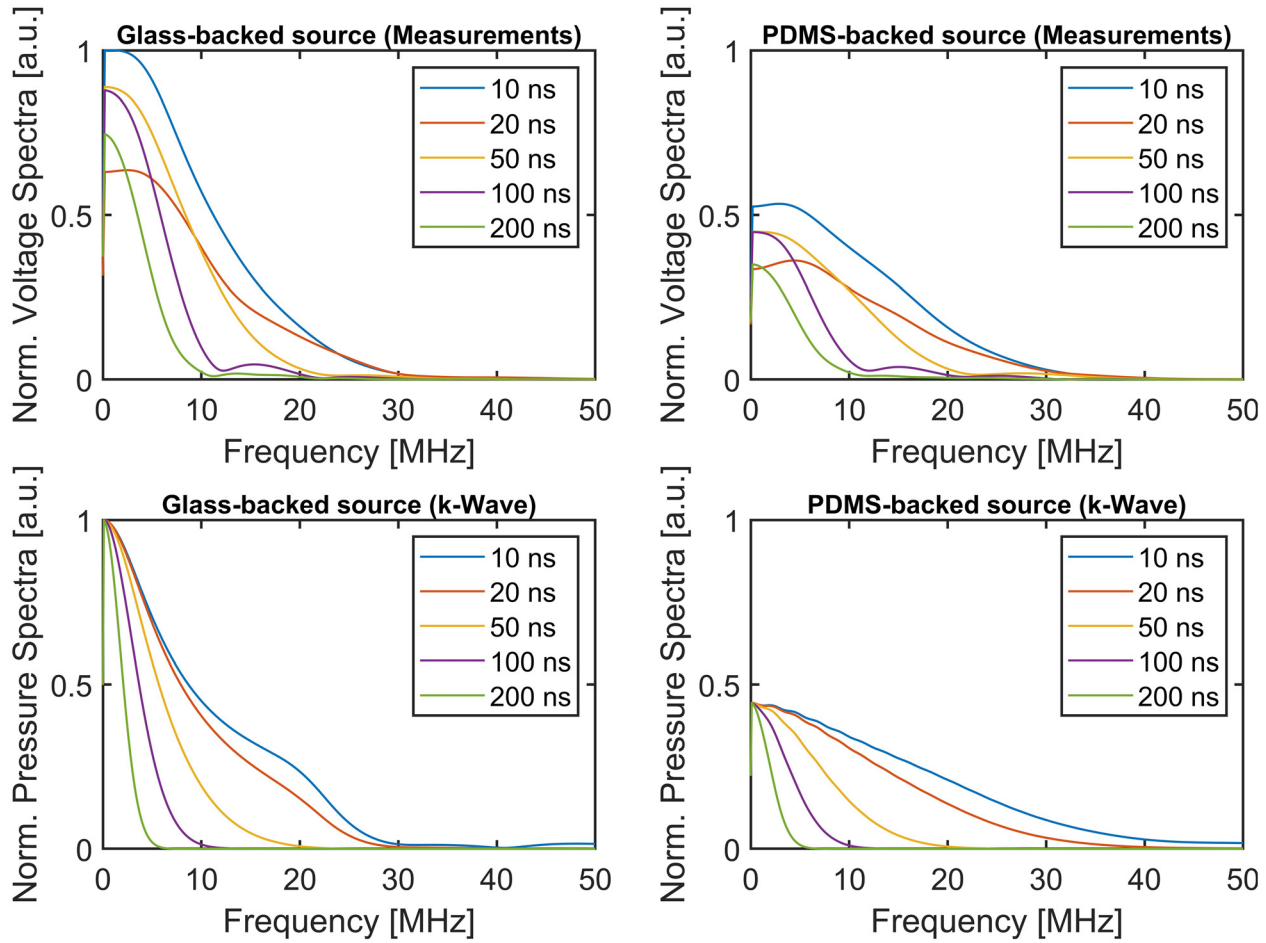


FIG. 4. (Color online) Frequency spectra of the measured voltage and simulated pressure time-series shown in Fig. 3 of glass-backed and PDMS-backed CPN sources. Before calculating the spectra, the measurement pulses were windowed using a Kaiser window (alpha = 9).

CPN source, and water. The time-series from the glass and PDMS-backed cases were recorded in the water medium one grid point outside the CPN medium. In step 2, the time-series recorded in step 1 were propagated through water. An additional advantage of splitting the model is that it allows the use of relevant reference sound-speed, c_{ref} for the k -space (dispersion-reducing) factor, which improves the convergence rate with the time step. In step 1 it is important to model the wave propagation most accurately within the CPN medium rather than glass or water so $c_{ref} = c_{CPN}$ was chosen. In step 2 since it is a homogeneous medium $c_{ref} = c_{water}$. A schematic of the simulation grid is shown in Fig. 7.

The time-series in step 1 were passed to step 2 using a time-varying “Dirichlet” source in which, at each time step and at the grid points where step 1 meets step 2, the acoustic pressure was replaced with the down-sampled time-series recorded in step 1. (With the use of such sources, it has previously been shown that the solution’s amplitude converged to within 3% of the actual solution.³⁰ The error arises because the data replacement at each time step does not preserve the spatial gradients that existed in the field at the previous time step. However, this is not a limiting factor in this work since the effect is the same for all simulations, and

here the ratio of the amplitudes for the glass and PDMS backings is the quantity of interest.)

In step 1, the grid spacing Δx was 125 nm, Δt was 167 fs, and c_{ref} was 945 m s^{-1} . In step 2, the recorded time-series were down-sampled and propagated in a water-only medium. The grid spacing Δx was 250 nm, Δt was 5 ps and c_{ref} was 1482.5 m s^{-1} . The thickness of the optically absorbing layer in the model was set to $22 \mu\text{m}$, which is an average of the source thicknesses of 20 and $24 \mu\text{m}$ used in the experiments. The spatial profile of the optical absorption in the CPN medium was defined as $p(x) = A \exp(-\mu x)$, where μ is the optical attenuation coefficient. The amplitude of $p(x)$ was set to $A = 250 \text{ kPa}$ for the glass-backed case and for the PDMS-backed case the amplitude was scaled down by 5% to account for optical absorption in the PDMS backing. Gaussian shaped pulses of full-width at half-maximum (FWHM) from 0.25 to 600 ns were used in the simulations. At each time step the spatial profile of the optical absorption energy was weighted by the Gaussian shaped time pulse and added to the pressure field on the grid (a time-varying source). The acoustic absorption in units of dB cm^{-1} of glass, PDMS, PDMS-based CPN film, and water are $0.0209f^{1.0758}$, $1.6f^{1.47}$, $1.17f^{1.61}$, and $0.00217f^2$, respectively, where f is in MHz.^{31–33} Since k-Wave requires the

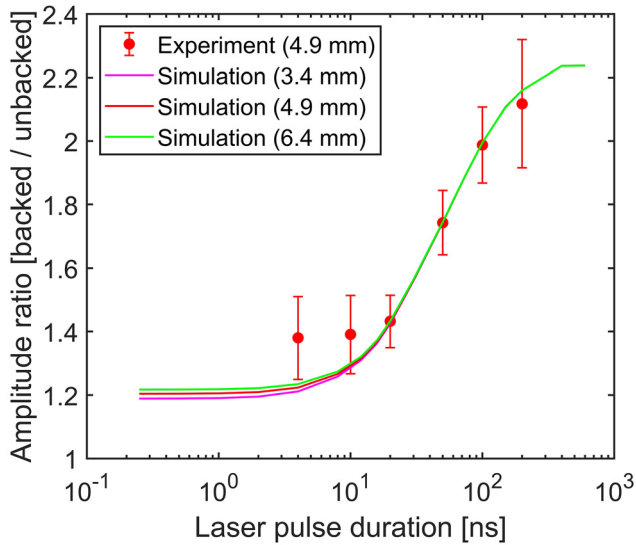


FIG. 5. (Color online) Ratios of glass-backed and PDMS-backed wave amplitudes for various laser pulse durations from stress confined ($\tau < d/c$) to unconfined ($\tau > d/c$) case. The error bars on the experimental ratios (red filled circles) represent standard deviation in the measured data obtained from two sets of glass-backed and PDMS-backed sources. Parenthetical entries in the plot legend are the distances from the CPN source at which the measurement or simulated time-series were recorded.

power law exponent of the acoustic absorption to be the same everywhere, it was set to the value for water, and the absorption coefficients in the different layers were varied by setting different pre-factors, an order of magnitude different for glass, PDMS, and PDMS-based CPN. The model input parameters are shown in Table III. The acoustic absorption of glass, CPN film, and the adjusted values based on the variation of water absorption values are shown in Fig. 8. Although there are differences in the two absorption values, overall, the absorption based on water values represents the

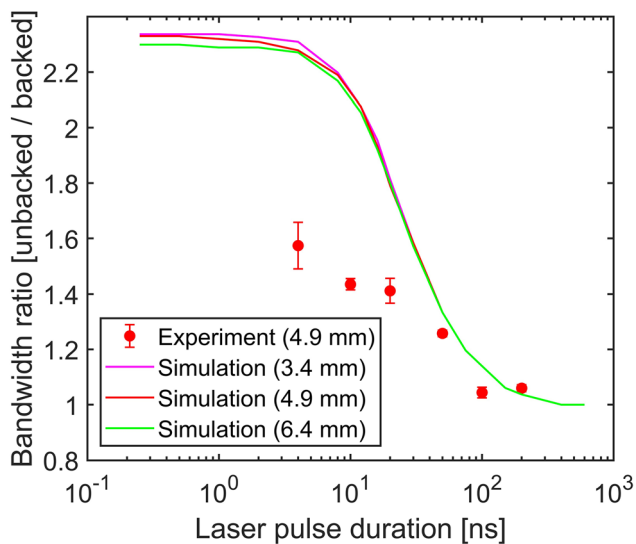
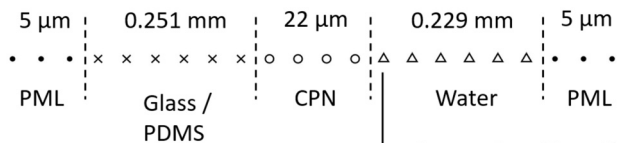


FIG. 6. (Color online) Ratios of -6 dB bandwidths calculated from the amplitude spectra of glass-backed and PDMS-backed CPN sources from experiment and numerical time-series. The error bars on the experimental ratios (red filled circles) represent standard deviation in the measured data.

Step 1:



Step 2:

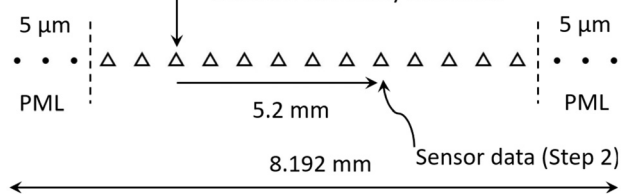


FIG. 7. Setup of the split numerical model to test the effect of CPN source backing for laser pulse durations from the stress confined ($\tau < d/c$) to the unconfined ($\tau > d/c$) cases. PML: Perfectly matched layer; CPN: Carbon-polymer nanocomposite. In step 1, the grid spacing Δx and time step Δt were 125 nm and 167 fs, respectively. The pressure time-series recorded in step 1 was down-sampled and introduced in step 2 as a time-varying Dirichlet boundary condition 0.2 mm away from PML on the left. In step 2, the Δx and Δt were 250 nm and 5 ps, respectively. The time-series were recorded at approximately three distances 3.4, 4.9, and 6.4 mm from the source.

type of acoustic loss at least in the CPN film, which is of interest. Simulations in step 2 were repeated, accounting for the nonlinearity of water although, as mentioned above, this made little difference.

The time-series recorded in step 2 (water-only model) at a distance of 4.9 mm from the location of the interior source is shown in Fig. 3. The five laser pulse durations 10, 20, 50, 100, and 200 ns corresponds to the tunable duration

TABLE III. Model input parameters used in a 1D simulation of the effect of glass and PDMS backing materials on LGUS from CPN films. Material properties data for sound-speed and mass density were obtained from Refs. 5, 6, and 34–36. The mass density and sound-speed of CPN film were assumed the same as that of PDMS. Furthermore, the mass-density and sound-speed of PDMS backing and CPN film were lowered by 10% of their nominal values to obtain closer agreement with experimental ratios (see Fig. 5).

| Parameter | Material | Value | Units |
|---|----------------|----------------------------|--------------------|
| Mass density, ρ_0 | Glass | 2230 | kg m^{-3} |
| | PDMS | 868 | |
| | Water | 998.2 | |
| Sound-speed, c_0 | Glass | 5640 | m s^{-1} |
| | PDMS | 945 | |
| | Water | 1482.5 | |
| Acoustic absorption, α (f^{β}) | Glass | $0.252 \times 10^{-6} f^2$ | Np m^{-1} |
| | PDMS | $252 \times 10^{-6} f^2$ | |
| | Water | $2.52 \times 10^{-6} f^2$ | |
| Optical attenuation coefficient, μ | PDMS-based CPN | 53 000 | m^{-1} |
| Stress-confined amplitude | — | 250 000 | Pa |

f is frequency in MHz.

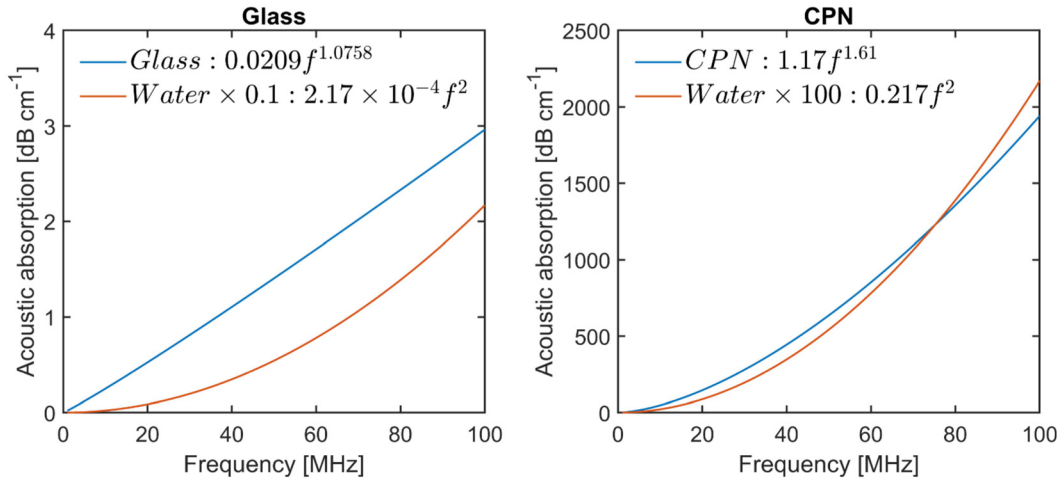


FIG. 8. (Color online) The acoustic absorption of glass (Ref. 32) and CPN-based PDMS film (Ref. 31) are plotted alongside the adjusted acoustic absorption used in the numerical simulation, which were obtained by varying the acoustic absorption of water values. In the legend entry, f , is frequency in MHz.

laser pulses used in the experiments in Sec. II. The time-series obtained for 10 ns laser pulse duration satisfies the stress-confinement criteria (calculated using values of μ and c_0 of PDMS listed in Table I). In both glass-backed and PDMS-backed time-series the broadening of the pressure pulses are seen with increasing laser pulse durations. However, their stress-confined pressure amplitudes are not the same, unlike the prediction from the analytical model.²⁰ The difference is due to the inclusion of acoustic absorption in CPN, as mentioned previously. The pressure pulses from the glass-backed source are longer due to reflection from the acoustically hard backing. Consequently, the preferential loss of high frequencies due to acoustic absorption leads to greater loss in the shorter PDMS-backed pressure pulses compared to the glass-backed case. Therefore, the amplitudes of glass-backed and PDMS-backed pressure pulses for $\tau < \tau_{ac}$ are not equal, as they would be if there were no absorption.

The variation of the ratio of the glass/PDMS-backed pressure amplitudes is plotted as a function of the pulse duration in Fig. 5, in Sec. II for comparison with the experimental measurements.

IV. CONCLUSIONS

In this article, it was shown experimentally that a planar laser-generated ultrasound source with a hard reflective backing will generate higher acoustic pressures than a comparable source with an acoustically matched backing when the stress confinement condition is not met. The explanation of the results was supported by numerical simulations. Thin carbon-polymer nanocomposite (CPN) sources with their thicknesses greater than their optical absorption depth were fabricated on glass backing (acoustically reflective) and polymer backing (acoustically matched) materials. An experimental tunable duration fibre-laser was used to investigate the laser-generated ultrasound pulses at select laser pulse durations spanning from stress confined to unconfined conditions. The generated ultrasound pulses were measured

using a broad-bandwidth Fabry–Pérot interferometric ultrasound sensor. These measurements were compared to a numerical model that is a generalisation of the analytical model. The ratios of the measured amplitudes from glass-backed over polymer-backed sources qualitatively agreed with the monotonic increase with laser pulse duration seen in the numerical model, which reached a limiting value that is dependent on the acoustic properties of the optical absorber and backing. Similarly, the ratios of -6 dB bandwidth of polymer-backed over glass-backed sources qualitatively agreed with the numerical model, which showed a monotonic decrease with laser pulse duration before reaching a limiting value. This is because, due to backing reflections, acoustic pulses generated from glass-backed sources are approximately twice as long as those generated from polymer-backed sources for short laser pulse durations, but for longer laser pulse durations the effect of backing reflections on acoustic pulse duration is proportionately small, and hence they contain similar frequency content.

ACKNOWLEDGMENTS

S.R. thanks the U.K. Department for Business, Energy & Industrial Strategy’s funding of the National Measurement System. Portions of this article come from the Ph.D. dissertation of S.R.²⁴ B.T.C. acknowledges the European Union’s Horizon 2020 research and innovation program H2020 ICT 2016–2017 under Grant Agreement No. 732411, which is an initiative of the Photonics Public Private Partnership, and EPSRC Grant No. EP/T014369/1. T.A. acknowledges the support from Engineering and Physical Sciences Research Council Grant No. EP/J022144/1. M.B., D.L., S.A., and D.R. acknowledge support from the Engineering and Physical Sciences Research Council Grant No. EP/J021970/1.

¹B. Cox, J. G. Laufer, S. R. Arridge, and P. C. Beard, “Quantitative spectroscopic photoacoustic imaging: A review,” *J. Biomed. Opt.* **17**(6), 061202 (2012).

- ²M. Ruiz-Veloz, G. Martínez-Ponce, R. I. Fernández-Ayala, R. Castro-Beltrán, L. Polo-Parada, B. Reyes-Ramírez, and G. Gutiérrez-Juárez, “Thermally corrected solutions of the one-dimensional wave equation for the laser-induced ultrasound,” *J. Appl. Phys.* **130**(2), 025104 (2021).
- ³W. Nunes dos Santos, P. Mummery, and A. Wallwork, “Thermal diffusivity of polymers by the laser flash technique,” *Polym. Test* **24**(5), 628–634 (2005).
- ⁴J. E. Mark, *Polymer Data Handbook*, 2nd ed. (Oxford University Press, Oxford, 2009).
- ⁵A. Cafarelli, A. Verbeni, A. Poliziani, P. Dario, A. Menciasci, and L. Ricotti, “Tuning acoustic and mechanical properties of materials for ultrasound phantoms and smart substrates for cell cultures,” *Acta Biomater.* **49**, 368–378 (2017).
- ⁶S. Rajagopal, T. Sainsbury, B. E. Treeby, and B. T. Cox, “Laser generated ultrasound sources using carbon-polymer nanocomposites for high frequency metrology,” *J. Acoust. Soc. Am.* **144**(2), 584–597 (2018).
- ⁷B. Y. Hsieh, J. Kim, J. Zhu, S. Li, X. Zhang, and X. Jiang, “A laser ultrasound transducer using carbon nanofibers-polydimethylsiloxane composite thin film,” *Appl. Phys. Lett.* **106**(2), 021902 (2015).
- ⁸H. Moon, H. Kim, D. Kumar, H. Kim, C. Sim, J. H. Chang, J. M. Kim, and D.-W. Lim, “Amplified photoacoustic performance and enhanced photothermal stability of reduced graphene oxide coated gold nanorods for sensitive photoacoustic imaging,” *ACS Nano* **9**(3), 2711–2719 (2015).
- ⁹S. Noimark, R. J. Colchester, B. J. Blackburn, E. Z. Zhang, E. J. Alles, S. Ourselin, P. C. Beard, I. Papakostantinou, I. P. Parkin, and A. E. Desjardins, “Carbon-nanotube-PDMS composite coatings on optical fibers for all-optical ultrasound imaging,” *Adv. Funct. Mater.* **26**(46), 8390–8396 (2016).
- ¹⁰S.-L. Chen, “Review of laser-generated ultrasound transmitters and their applications to all-optical ultrasound transducers and imaging,” *Appl. Sci* **7**(1), 25 (2016).
- ¹¹C. Moon, X. Fan, K. Ha, and D. Kim, “Generation of planar blast waves using carbon nanotubes-poly-dimethylsiloxane optoacoustic transducer,” *AIP Adv.* **7**(1), 015107 (2017).
- ¹²T. Lee, H. W. Baac, Q. Li, and L. J. Guo, “Efficient photoacoustic conversion in optical nanomaterials and composites,” *Adv. Opt. Mater* **6**(24), 1800491 (2018).
- ¹³E. Aytac-Kiperçil, A. E. Desjardins, B. E. Treeby, S. Noimark, I. P. Parkin, and E. J. Alles, “Modelling and measurement of laser-generated focused ultrasound: Can interventional transducers achieve therapeutic effects?,” *J. Acoust. Soc. Am.* **149**(4), 2732–2742 (2021).
- ¹⁴H. W. Baac, T. Lee, and L. J. Guo, “Micro-ultrasonic cleaving of cell clusters by laser-generated focused ultrasound and its mechanisms,” *Biomed. Opt. Express* **4**(8), 1442–1450 (2013).
- ¹⁵S. Manohar and D. Razansky, “Photoacoustics: A historical review,” *Adv. Opt. Photon.* **8**(4), 586–617 (2016).
- ¹⁶S. Rajagopal and B. T. Cox, “100 MHz bandwidth planar laser-generated ultrasound source for hydrophone calibration,” *Ultrasonics* **108**, 106218 (2020).
- ¹⁷G. J. Diebold, “Chapter 1 photoacoustic monopole radiation: Waves from objects with symmetry in one, two, and three dimensions,” in *Photoacoustic Imaging and Spectroscopy*, 1st ed., edited by L. V. Wang, (CRC Press, Boca Raton, FL, 2009), p. 536.
- ¹⁸S. M. Park, M. I. Khan, H. Z. Cheng, and G. J. Diebold, “Photoacoustic effect in strongly absorbing fluids,” *Ultrasonics* **29**(1), 63–67 (1991).
- ¹⁹S. Rajagopal, B. E. Treeby, and B. T. Cox, “Effect of backing on carbon-polymer nanocomposite sources for laser generation of broadband ultrasound pulses,” in *2018 IEEE International Ultrasonics Symposium (IUS)* (IEEE, New York, 2018), pp. 1–4.
- ²⁰S. Rajagopal and B. T. Cox, “Modelling laser ultrasound waveforms: The effect of varying pulse duration and material properties,” *J. Acoust. Soc. Am.* **149**(3), 2040–2054 (2021).
- ²¹T. J. Allen, M. Berendt, D. Lin, S. U. Alam, N. T. Huynh, E. Zhang, D. J. Richardson, and P. C. Beard, “High pulse energy fibre laser as an excitation source for photoacoustic tomography,” *Opt. Express* **28**(23), 34255–34265 (2020).
- ²²E. Zhang, J. Laufer, and P. Beard, “Backward-mode multiwavelength photoacoustic scanner using a planar Fabry-Perot polymer film ultrasound sensor for high-resolution three-dimensional imaging of biological tissues,” *Appl. Opt.* **47**(4), 561–577 (2008).
- ²³A. M. Hurrell and S. Rajagopal, “The practicalities of obtaining and using hydrophone calibration data to derive pressure waveforms,” *IEEE Trans. Ultrason. Ferroelectr. Freq. Control* **64**(1), 126–140 (2017).
- ²⁴S. Rajagopal, *Laser-Generated, Plane-Wave, Broadband Ultrasound Sources for Metrology* (University College London, London, 2020).
- ²⁵M. Polyanskiy, “RefractiveIndex.INFO,” (2018), <https://refractiveindex.info/?shelf=main&book=Al&page=Rakic> (Last viewed 3 February 2019).
- ²⁶B. T. Cox, J. G. Laufer, K. P. Kostli, and P. C. Beard, “Experimental validation of photoacoustic k-space propagation models,” in *SPIE Proceedings Vol. 5320, Photons Plus Ultrasound: Imaging and Sensing*, edited by A. A. Oraevsky and L. V. Wang (International Society for Optics and Photonics, Bellingham, WA, 2004), pp. 238–248.
- ²⁷B. E. Treeby and B. T. Cox, “k-Wave: MATLAB toolbox for the simulation and reconstruction of photoacoustic wave fields,” *J. Biomed. Opt.* **15**(2), 021314 (2010).
- ²⁸B. E. Treeby, J. Jaros, A. P. Rendell, and B. T. Cox, “Modeling nonlinear ultrasound propagation in heterogeneous media with power law absorption using a k-space pseudospectral method,” *J. Acoust. Soc. Am.* **131**(6), 4324–4336 (2012).
- ²⁹B. E. Treeby and B. T. Cox, “Modeling power law absorption and dispersion for acoustic propagation using the fractional Laplacian,” *J. Acoust. Soc. Am.* **127**(5), 2741–2748 (2010).
- ³⁰B. Treeby, F. Lucka, E. Martin, and B. T. Cox, “Equivalent-source acoustic holography for projecting measured ultrasound fields through complex media,” *IEEE Trans. Ultrason. Ferroelectr. Freq. Control* **65**(10), 1857–1864 (2018).
- ³¹E. J. Alles, J. Heo, S. Noimark, R. J. Colchester, I. P. Parkin, H. W. Baac, and A. E. Desjardins, “Acoustical characterisation of carbon nanotube-loaded polydimethylsiloxane used for optical ultrasound generation,” in *2017 IEEE International Ultrasonics Symposium (IUS)* (IEEE, Piscataway, NJ, 2017), pp. 1–4.
- ³²A. Slotwinski, “Ultrasonic testing,” in *Handbook of Reference Data for NonDestructive Testing*, edited by L. Mordfin (ASTM International, West Conshohocken, PA, 2002), pp. 31–48.
- ³³J. M. M. Pinkerton, “The absorption of ultrasonic waves in liquids and its relation to molecular constitution,” *Proc. Phys. Soc. B* **62**(2), 129–141 (1949).
- ³⁴Dow Chemical Company, “SYLGARD 84 Silicone Elastomer” (2017), <https://consumer.dow.com/content/dam/dcc/documents/en-us/productdata/tasheet/11/11-31/11-3184-sylgard-184-elastomer.pdf?iframe=true%0A> (Last viewed 30 March 2019).
- ³⁵Kaye & Laby, “Mechanical properties of materials. 2.2.1 Densities,” online version 1.1 (2008), https://web.archive.org/web/20190422110321/http://www.kayelaby.npl.co.uk/general_physics/2_2/2_2_1.html (Last viewed 29 December 2022).
- ³⁶Kaye & Laby, “Acoustics. 2.4.1: The speed and attenuation of sound,” online version 1.0 (2005), https://web.archive.org/web/20190508003406/http://www.kayelaby.npl.co.uk/general_physics/2_4/2_4_1.html (Last viewed 29 December 2022).